

1 **Ultra-deep sequencing differentiates patterns of skin clonogenic mutations associated**  
2 **with sun-exposure status and skin cancer risk**

3  
4 **Classification:** Biological Sciences, Genetics; Cancer risk; Early detection;

5  
6 Lei Wei<sup>1,\*§</sup>, Sean R. Christensen<sup>2,\*</sup>, Megan Fitzgerald<sup>3</sup>, James Graham<sup>1</sup>, Nicholas Hutson<sup>1</sup>, Chi  
7 Zhang<sup>4</sup>, Ziyun Huang<sup>5</sup>, Qiang Hu<sup>1</sup>, Fenglin Zhan<sup>1,6</sup>, Jun Xie<sup>7</sup>, Jianmin Zhang<sup>8</sup>, Song Liu<sup>1</sup>, Eva  
8 Remenyik<sup>9</sup>, Emese Gellen<sup>9</sup>, Oscar R. Colegio<sup>10,11</sup>, Michael Bax<sup>10</sup>, Jinhui Xu<sup>12</sup>, Haifan Lin<sup>13</sup>, Wendy  
9 J. Huss<sup>14,\*</sup>, Barbara A. Foster<sup>14,\*</sup>, Gyorgy Paragh<sup>3,9,\*§</sup>

10 **Author affiliations:**

11 <sup>1</sup>Department of Biostatistics and Bioinformatics, Roswell Park Comprehensive Cancer Center,  
12 Buffalo, NY

13 <sup>2</sup>Department of Dermatology, Yale University School of Medicine, New Haven, CT

14 <sup>3</sup>Department of Cell Stress Biology, Roswell Park Comprehensive Cancer Center, Buffalo, NY

15 <sup>4</sup>School of Biological Sciences Center for Plant Science and Innovation, University of Nebraska,  
16 Lincoln, NE

17 <sup>5</sup>Department of Computer Science and Software Engineering, Penn State Erie, The Behrend  
18 College

19 <sup>6</sup>PET/CT center, The First Affiliated Hospital of USTC, Division of Life Sciences and Medicine,  
20 University of Science and Technology of China, Hefei, Anhui, 230001, P.R. China

21 <sup>7</sup>Department of Statistics, Purdue University, West Lafayette, IN

22 <sup>8</sup>Department of Cancer Genetics and Genomics, Roswell Park Comprehensive Cancer Center,  
23 Buffalo, NY

24 <sup>9</sup>Department of Dermatology, Faculty of Medicine, University of Debrecen, Debrecen, Hungary

25 <sup>10</sup>Department of Dermatology, Roswell Park Comprehensive Cancer Center, Buffalo, NY

26 <sup>11</sup>Department of Immunology, Roswell Park Comprehensive Cancer Center, Buffalo, NY

27 <sup>12</sup>Department of Computer Science and Engineering, State University of New York at Buffalo

28 <sup>13</sup>Yale Stem Cell Center, Yale University School of Medicine, New Haven, CT

29 <sup>14</sup>Department of Pharmacology and Therapeutics, Roswell Park Comprehensive Cancer Center,  
30 Buffalo, NY

31

32 \* These authors contributed equally

33 § Corresponding authors: [Lei.Wei@RoswellPark.org](mailto:Lei.Wei@RoswellPark.org) and [Gyorgy.Paragh@RoswellPark.org](mailto:Gyorgy.Paragh@RoswellPark.org)

34

35 **Email addresses:**

36 LW: [Lei.Wei@RoswellPark.org](mailto:Lei.Wei@RoswellPark.org)

37 SC: [Sean.Christensen@Yale.edu](mailto:Sean.Christensen@Yale.edu)

38 MF: [Megan.Fitzgerald@RoswellPark.org](mailto:Megan.Fitzgerald@RoswellPark.org)

39 JG: [james.graham@stonybrookmedicine.edu](mailto:james.graham@stonybrookmedicine.edu)

40 NH: [ndhutso@gmail.com](mailto:ndhutso@gmail.com)

41 CZ: [czhang5@unl.edu](mailto:czhang5@unl.edu)

42 ZH: [zxh201@psu.edu](mailto:zxh201@psu.edu)

43 QH: [qiang.hu@roswellpark.org](mailto:qiang.hu@roswellpark.org)

44 FZ: [zhan209@hotmail.com](mailto:zhan209@hotmail.com)

45 JX: [junxie@purdue.edu](mailto:junxie@purdue.edu)

46 JZ: [jianmin.zhang@roswellpark.org](mailto:jianmin.zhang@roswellpark.org)

47 SL: [song.liu@roswellpark.org](mailto:song.liu@roswellpark.org)

48 ER: [remenyik@med.unideb.hu](mailto:remenyik@med.unideb.hu)  
49 EG: [emesegellen@med.unideb.hu](mailto:emesegellen@med.unideb.hu)  
50 OC: [Oscar.Colegio@RoswellPark.org](mailto:Oscar.Colegio@RoswellPark.org)  
51 MB: [Michael.Bax@RoswellPark.org](mailto:Michael.Bax@RoswellPark.org)  
52 JX: [jinhui@buffalo.edu](mailto:jinhui@buffalo.edu)  
53 HL: [haifan.lin@yale.edu](mailto:haifan.lin@yale.edu)  
54 WJH: [Wendy.Huss@RoswellPark.org](mailto:Wendy.Huss@RoswellPark.org)  
55 BAF: [Barbara.Foster@RoswellPark.org](mailto:Barbara.Foster@RoswellPark.org)  
56 GP: [Gyorgy.Paragh@RoswellPark.org](mailto:Gyorgy.Paragh@RoswellPark.org)

57

58 **Keywords:** ultraviolet light, clonogenic mutation, photocarcinogenesis, sun exposure, ultra-  
59 deep sequencing, skin cancer risk

60

61 **Abstract**

62 Non-melanoma skin cancer is the most common human malignancy and is primarily caused by  
63 exposure to ultraviolet (UV) radiation. The earliest detectable precursor of UV-mediated skin  
64 cancer is the growth of cell groups harboring clonal mutation (CM) in clinically normal appearing  
65 skin. Systematic evaluation of CMs is crucial to understand early photo-carcinogenesis. Previous  
66 studies confirmed the presence of CMs in sun-exposed skin. However, the relationship between  
67 UV-exposure and the accumulation of CMs, and the correlation of CMs with skin cancer risk  
68 remain poorly understood. To elucidate the exact molecular and clinical effects of long-term UV-  
69 exposure on skin, we performed targeted ultra-deep sequencing in 450 individual-matched sun-  
70 exposed (SE) and non-sun-exposed (NE) epidermal punch biopsies obtained from clinically  
71 normal skin from 13 donors. A total of 638 CMs were identified, including 298 UV-signature  
72 mutations (USMs). The numbers of USMs per sample were three times higher in the SE samples  
73 and were associated with significantly higher variant allele frequencies (VAFs), compared with  
74 the NE samples. We identified genomic regions in *TP53*, *NOTCH1* and *GRM3* where mutation  
75 burden was significantly associated with UV-exposure. Six mutations were almost exclusively  
76 present in SE epidermis and accounted for 42% of the overall difference between SE and NE  
77 mutation burden. We defined Cumulative Relative Clonal Area (CRCA), a single metric of UV-  
78 damage calculated by the overall relative percentage of the sampled skin area affected by CMs.  
79 The CRCA was dramatically elevated by a median of 11.2 fold in SE compared to NE samples.  
80 In an extended cohort of SE normal skin samples from patients with a high- or low- burden of  
81 cutaneous squamous cell carcinoma (cSCC), the SE samples in high-cSCC patients contained  
82 significantly more USMs than SE samples in low-cSCC patients, with the difference mostly  
83 conferred by mutations from low-frequency clones (defined by  $VAF \leq 1\%$ ) but not expanded clones  
84 ( $VAF > 1\%$ ). Our studies of differential mutational features in normal skin between paired SE/NE

85 body sites and high/low-cSCC patients provide novel insights into the carcinogenic effect of UV  
86 exposure, and suggest CMs might be used to develop novel biomarkers for predicting cancer risk.

## 87 **Significance statement:**

88 In UV radiation exposed skin, mutations fuel clonal cell growth. We established a sequencing-  
89 based method to objectively assess the mutational differences between sun-exposed (SE) and  
90 non-sun-exposed (NE) areas of normal human skin. Striking differences, in both the numbers of  
91 mutations and variant allele frequencies, were found between SE and NE areas. Furthermore, we  
92 identified specific genomic regions where mutation burden is significantly associated with UV-  
93 exposure status. These findings revealed previously unknown mutational patterns associated with  
94 UV-exposure, providing important insights into UV radiation's early carcinogenic effects.  
95 Additionally, in an extended cohort, we identified preliminary association between normal skin  
96 mutation burden and cancer risk. These findings pave the road for future development of  
97 quantitative measurement of subclinical UV damage and skin cancer risk.

## 98 **Background**

99 Ultraviolet (UV) light is responsible for over 5 million cases of skin cancer annually in the US,  
100 which is more human malignancies than all other environmental carcinogens combined<sup>1,2</sup>. In  
101 mammals, nucleotide excision repair eliminates UV-mediated DNA lesions, but this mechanism  
102 of repair is error prone resulting in frequent mutations<sup>3</sup>. The preferential location of UVB induced  
103 DNA lesions results in a specific pattern of so-called UV signature mutations at dipyridine sites  
104 (C>T, CC>TT)<sup>4</sup>. In most skin cancers, including cutaneous squamous cell carcinoma (cSCC), the  
105 burden of UV signature driver mutations is high<sup>4,5</sup>. While some cSCC arise from visible  
106 precancerous lesions known as actinic keratoses (AKs), many cSCC arise in apparently "normal"  
107 skin areas from precursors that are clinically invisible<sup>6</sup>. Therefore, clinically visible precursors are  
108 an ominous sign but not a sensitive early measure of photocarcinogenesis.

109 *TP53* mutations are among the most common driver mutations in cSCC, and are also detected  
110 by immunohistochemistry in aged normal skin<sup>7,8</sup>. These UV-induced *TP53* mutations facilitate  
111 clonal expansion of cells harboring them and therefore behave as early clonogenic mutations  
112 (CMs)<sup>9</sup>. For two decades *TP53* mutant keratinocyte cell clones were considered the earliest  
113 manifestations of skin carcinogenesis<sup>7,8,10</sup>. Because p53 clonal immunopositivity could not be  
114 efficiently quantified in human skin, detection of mutant *TP53* for assessment of  
115 photocarcinogenesis in clinical dermatology practice has been unattainable. The low relative  
116 abundance of clonal DNA previously limited efficient detection of early mutated cell groups.  
117 However, with improved high throughput sequencing technology we have finally reached the  
118 lower end of this threshold and efficient detection of rare mutations in normal tissue is becoming  
119 feasible in recent studies by others and us using deep bulk sequencing or single cell DNA  
120 sequencing<sup>11-16</sup>. In exploratory analyses, CMs were found to be abundant in clinically normal skin  
121 from sun-exposed sites in *NOTCH1*, *NOTCH2*, *FAT1* and several other genes besides *TP53*<sup>12</sup>.  
122 Prior attempts to establish a quantitative method for assessing photodamage and skin cancer risk  
123 had limited success<sup>17,18</sup>. A method that enables quantitative evaluation of early photodamage is  
124 expected to help optimize personalized sun-protective measures and may also serve as a tool for  
125 assessing the need and efficacy of early preventative treatment interventions.

126 In the current work we developed an ultra-deep sequencing-based method to identify CMs in  
127 clinically normal epidermis and show differences in CMs between sun-exposed and non-sun-  
128 exposed skin areas. We then correlated CMs with skin cancer burden in another independent  
129 cohort of cSCC patients and found mutational features in normal skin are significantly associated  
130 with cancer burden.

131

132 **Methods**

133 **Samples:**

134 A total of 464 normal human skin samples were collected from 13 Caucasian post-mortem donors  
135 over the age of 55 years using Roswell Park's Rapid Tissue Acquisition Program under a Roswell  
136 Park approved IRB protocol within 24 hours of death from frequently sun-exposed (SE) sites (left  
137 dorsal forearm) and non-sun-exposed (NE) sites (left medial buttock). Exclusion criteria included  
138 any visible skin abnormalities in the tissue areas. Eligible donors were identified and clinically  
139 normal appearing skin was harvested. Skin samples were kept in tissue preservation medium,  
140 Belzer UW cold storage solution (Bridge to Life, USA) at 4°C until processed. All samples that  
141 could be processed within 36 hours or less after death were included in the study. The mean age  
142 of the donors was 72.3 years (SD:  $\pm 8.2$  years; range 60-80 years). The male to female gender  
143 ratio was 7:6, and 12/13 donors had no history of skin cancer.

144 The adipose tissue was removed from each human skin sample using sterile scissors. The  
145 samples were cut into strips wide enough to harvest 6 mm punches. The epidermis was separated  
146 from the dermis by placing the strips in tubes containing 10 ml of 5U/ml Dispase II (Stem Cell  
147 Technologies, USA) and incubated at 4°C overnight and at 37°C for 2-3 hours. After Dispase  
148 digestion the specimens were placed in a petri dish containing a small amount of 1x DPBS  
149 (Corning, USA) and using sterile tweezers, the epidermis was carefully removed from the dermis.  
150 Using disposable biopsy punches, 1, 2, 3, 4 and 6 mm diameter epidermal pieces were taken  
151 from the epidermal sheets and punched epidermal pieces were placed into a sterile 1.5 mL vials.  
152 In addition to the epidermal punches, large bulk pieces of dermis were also removed from the  
153 skin samples using a disposable #15 blade and placed into a sterile 1.5 mL vial for use as a  
154 germline control.

155 For the extended cohort of the study, 20 human skin samples were obtained in a de-identified  
156 manner from 8 undergoing surgery for cSCC. The study was granted exemption by the Yale  
157 University Human Investigation Committee (Protocol 1509016421). All individuals had biopsy-  
158 confirmed cSCC that was completely excised by Mohs micrographic surgery with intraoperative  
159 histologic verification of clear surgical margins. Immediately following excision of cSCC, adjacent  
160 normal skin was excised to facilitate surgical repair and samples for sequencing were immediately  
161 harvested. From each individual, two skin samples at a fixed linear distance from the cSCC were  
162 obtained from the adjacent, sun-exposed, normal skin. One sample was obtained at a distance  
163 of 1mm from the cSCC surgical margin, and one at a distance of 6mm from the surgical margin.  
164 From four patients, a tumor sample from grossly visible cSCC was also obtained at the time of  
165 surgery. All samples were obtained with a 2mm punch biopsy to a depth of approximately 1 mm,  
166 including epidermis and superficial dermis.

167 **DNA isolation:**

168 DNA samples from the primary cohort were extracted using Purelink™ Genomic DNA mini kit  
169 (Invitrogen, USA). Epidermal samples were digested using Proteinase K at 55°C heating block  
170 overnight following the manufacturers recommendations. For the extended cohort of samples,  
171 skin biopsies were similarly digested using Proteinase K and DNA was purified with phenol-  
172 chloroform extraction and ethanol precipitation. DNA was eluted with 28 µL of Molecular Biology  
173 Grade Water (Corning, USA) for 1 and 2 mm punches or 36 µL of Molecular Biology Grade Water  
174 for 3, 4, and 6 mm punches. The isolated genomic DNA was stored at -20°C and the DNA  
175 concentration of each extraction was measured using a Qubit fluorometer or Quanti-iT PicoGreen  
176 kit (Invitrogen, USA).

177 **Ultra-deep Targeted Sequencing:**

178 The sequencing libraries were generated using the TruSeq Custom Amplicon kit (Illumina, USA)  
179 using 10-50 ng of gDNA. Amplicons of ~150bp (primary cohort) or ~250bp (extended cohort) in  
180 length were designed using Illumina Design Studio Software. Custom oligo capture probes that  
181 flank the regions of interest were hybridized to the gDNA. A combined extension/ligation reaction  
182 completed the region of interest between these flanking custom oligo probes. PCR was then  
183 performed to add indices and sequencing adapters. The amplified final libraries were cleaned up  
184 using AmpureXP beads (Beckman Coulter). Purified libraries were run on a TapeStation  
185 DNA1000 screentape chip to verify desired size distribution, quantified by KAPA qPCR (KAPA  
186 Biosystems) and pooled equal molar in a final concentration of 2 nM. Pooled libraries were loaded  
187 on an Illumina HiSeq Rapid Mode V2 flow cell following standard protocols for 2x100 cycle  
188 sequencing (primary cohort), or Illumina NextSeq for 2x150 cycle sequencing (extended cohort).

189 **Bioinformatics analysis:**

190 High quality paired-end reads passing Illumina RTA filter were initially processed against the NCBI  
191 human reference genome (GRCh37) using public available bioinformatics tools <sup>19,20</sup>, and Picard  
192 (<http://picard.sourceforge.net/>). The coverage quality control required at least 80% of the targeted  
193 region covered by a minimum of 1,000X coverage. Putative mutations, including single nucleotide  
194 variants (SNVs) and small insertions/deletions (Indels), were initially identified by running variation  
195 detection module of Strelka<sup>21</sup> on each SE or NE epidermis sample paired with the matched dermal  
196 sample. From the detected SNVs, dinucleotide variants (DNV) or cluster of single nucleotide  
197 variants (CSNV) were recognized by running Multi-Nucleotide Variant Annotation Corrector (MAC)  
198 <sup>22</sup> on the original sequences. The putative mutations detected from all samples were consolidated  
199 into a list of unique mutations. Every unique mutation was re-visited in all samples to calculate  
200 the numbers of mutant/wildtype reads, as well as variant allele frequency (VAF) in each sample  
201 as previously described <sup>13</sup>.



202 To distinguish mutations from background errors, we modelled each mutation's background  
203 error rate distributions using VAFs from all control (dermal) samples. For each mutation, we  
204 started by fitting a *Weibull* distribution to VAFs from all control samples following a previously  
205 published method<sup>23</sup>, then every SE or NE epidermal sample's VAF was compared to the fitted  
206 distribution. A positive sample was defined as the sample's VAF of a mutation was significantly  
207 above background ( $p < 0.05$ , after Bonferroni correction). In the extended cohort where the control  
208 samples were not available, we adapted a dynamic control strategy, based on the assumption  
209 that any somatic mutation cannot be recurrent in more than 10% of all samples at the same site.  
210 In the previous primary cohort, all recurrent mutations were within 5% of all samples. For each  
211 potential mutation, we first cluster the VAFs of the mutation in all samples. Subsequently started  
212 from the cluster with lowest VAF, we transferred all samples of each cluster to the control cohort  
213 until at least 90% of all samples are in the control cohort. After mutation calling, all identified  
214 mutations including SNVs, DNVs, CSNVs and Indels were annotated using a customized program  
215 with NCBI RefSeq database.

216 Cumulative Relative Clonal Area (CRCA), defined as the overall percentage of biopsied skin  
217 area covered by UV-signature mutations (USMs) in a patient skin punch, was calculated as  
218 following:

$$219 \quad CRCA = \frac{\sum_{i=1}^n \sum_{j=1}^{m_i} (\pi r_i^2 * 2VAF_j)}{\sum_{i=1}^n \pi r_i^2}$$

220 with  $n$  = the total number of punches collected in the patient;  $r_i$  = the size (radius) of each punch;  
221  $m_i$  = the number of mutations in punch  $i$ ;  $VAF_j$  = the variant allele fraction of a specific mutation  $j$ .  
222 Here, the calculation of CRCA was based on the assumption that all mutations occur in one  
223 chromosome of regular diploid genomic regions. Additionally, although we did not consider the

224 situation when multiple mutations occur in the same cell, we did identify mutations that occur on  
225 the same reads and combined them into one mutation using MAC<sup>22</sup>.

## 226 **Statistics:**

227 The overall mutation numbers and VAFs between two groups, including SE and NE in the primary  
228 cohort, and the high- and low- cSCC burden in the extended cohort, were evaluated using a  
229 Wilcoxon test. Group-specific markers, including mutations, genes, regions and signatures were  
230 identified using a Fisher's exact test where the two variables in the contingency table were the  
231 samples' sun-exposure status (SE vs NE, in cohort #1) or cSCC burden (high vs low, in cohort  
232 #2) and mutational status. Multiple testing correction was implemented using the FDR approach  
233 as indicated.

## 234 **Results**

### 235 **Ultra-deep sequencing of epidermal samples using customized focused panels**

236 To generate a focused sequencing panel, targeting the most commonly mutated sequences in  
237 normal human skin, we selected an area of focus based on a previous dataset<sup>12</sup>. All previous  
238 mutations were assigned to 100 bp genomic segments. After sorting the segments by number of  
239 mutations, we designed a panel to capture the top 55 most frequently mutated segments from 12  
240 genes (5.5 kb in total, **Table S1**). The majority (65%) of the targeted segments came from the  
241 following 3 genes: *NOTCH1*, *NOTCH2*, and *TP53*. When summarized by coding regions, 79% of  
242 the targeted segments lie in protein coding regions, and the remaining segments were mostly in  
243 introns. In the previous dataset<sup>12</sup>, 87% of the samples harbored at least one mutation within this  
244 panel.

245 The primary cohort was sequenced using the focused panel in two batches. We first  
246 sequenced a discovery cohort of 374 human skin samples from 13 post-mortem donors: 360

247 epidermal samples, equally acquired from both sun-exposed (SE) and non-sun-exposed regions  
248 (NE) using 1 mm, 2 mm, 3 mm, 4 mm or 6 mm punch sizes. From the same 13 donors, DNA  
249 from bulk NE dermis (n=14, 1 donor contributed 2 samples) was isolated for germline controls.  
250 After initial analysis to determine the optimal punch size, we then tested a separate validation  
251 cohort of 90 epidermal samples from 9 of the 13 donors using the most effective punch size (2  
252 mm, as detailed in results “Optimization of punch size for USM detection”). In total, the dataset  
253 contains 464 samples: 225 SE, 225 NE, and 14 dermal samples as controls (**Table 1**) from 13  
254 individuals. After sequencing, 85% of samples reached a minimum of 10,000X coverage in at  
255 least 80% of the targeted region. The median of average coverage across all samples was  
256 64,730X (**Table S2a**), with only one sample exclusion (NE sample) due to sequencing failure.

257 To better define the clinical relevance of CMs, we sequenced an extended cohort of sun-  
258 exposed skin samples from human patients with cSCC. Twenty 2mm punch biopsy specimens  
259 were obtained from surgically excised skin from 8 individuals, including 16 normal skin samples  
260 and 4 samples of cSCC. For this extended cohort, a custom sequencing panel was designed to  
261 encompass the complete protein coding region of 12 genes with frequently reported mutations in  
262 UV-exposed skin (*NOTCH1*, *NOTCH2*, *NOTCH3*, *TP53*, *CDKN2A*, *BRAF*, *HRAS*, *KRAS*, *NRAS*,  
263 *KNSTRN*, *FAT1*, and *FGFR3*), and 1 control gene without expected functional significance in skin  
264 (*VHL*). This sequencing panel encompassed 59.5 kb. After sequencing, all samples have at least  
265 80% of the targeted region covered by a minimum of 10,000X coverage. The median value of  
266 average coverages across all samples was 47,158X (**Table S2b**).

### 267 **Delineate the mutational patterns associated with UV exposure**

268 To identify the mutations solely caused by UV exposure, we characterized the mutational profiles  
269 of individual-matched SE/NE epidermal samples. Additionally, we compared the epidermal  
270 samples to patient-matched dermal samples followed by an in silico error suppression to remove  
271 germline polymorphisms and low-frequency technical artifacts. Dinucleotide and other complex

272 mutations were identified by re-visiting the raw reads using a program that we previously  
273 developed<sup>22</sup>. Altogether, a total of 638 mutations were identified, predominantly single nucleotide  
274 variants (SNVs, n = 614 or 96.2%) or dinucleotide variants (DNVs, n = 20 or 3.1%) (**Table S3**).  
275 The median variant allele frequency (VAF) of all mutations was 2.1% (range 0.1% - 36.6%), and  
276 only 3% mutations reached a VAF greater than 10%.

277 Among the 55 targeted genomic segments, mutations were detected in 50 segments with an  
278 average of 7.1 and 4.7 mutations per segment in SE and NE samples, respectively (**Figure 1a**).  
279 Two segments were significantly (FDR  $p < 0.001$ ) associated with UV-exposure status,  
280 approximately corresponding to *TP53* amino acids 227-261 ("*TP53-3*", mutations in SE/NE = 38/0)  
281 and *NOTCH1* p.449-481 ("*NOTCH1-9*", mutations in SE/NE = 30/4). Interestingly, mutations in  
282 an adjacent region in *NOTCH1* p.419-449 ("*NOTCH1-10*") were not associated with UV exposure  
283 (mutations in SE/NE=48/40), even though "*NOTCH1-10*" was the most frequently mutated  
284 segment in the current study. Additionally, mutations were marginally enriched in SE samples  
285 (FDR  $p < 0.1$ ) in three other segments: two in *NOTCH1* ("*NOTCH1-14*" and "*NOTCH1-19*") and  
286 one in *GRM3* ("*GRM3-2*"). On the gene level, mutations in SE samples were only significantly  
287 enriched in *TP53* (FDR  $p < 0.001$ ), and marginally significant in *GRM3* (FDR  $p < 0.1$ ). Overall, the  
288 numbers of mutations in SE samples were 6.3 times higher than NE samples in *TP53*, and 4.3  
289 times in *GRM3* (**Figure 1b**). Mutations identified in nine other genes did not exhibit significant  
290 association with sun-exposure status either on the gene- or segment- level: *NOTCH2*, *ARID1A*,  
291 *SALL1*, *SCN1A*, *ERBB4*, *FAT4*, *FGFR3*, *ADGRB3* and *PPP1R3A*. These findings strongly  
292 suggest a highly genomic-region-specific pattern of the accumulation of UV-induced somatic  
293 mutations.

294 We next investigated potential hotspots and mutations associated with UV-exposure. After  
295 sorting all mutations by their genomic locations, one specific region in *TP53* (p.217-280),  
296 appeared to be "mutation exempt" in comparison to surrounding regions in NE samples. In

297 contrast, this region was highly mutated in SE samples (**Figure 2a**). We reanalyzed a recent study  
298 involving RNASeq of both SE and NE normal skin samples<sup>11</sup>, and found four mutations in this  
299 region, all from SE samples (**Table S4**). To identify mutations associated with UV exposure, we  
300 focused on highly recurrent mutations (present in  $\geq 5$  samples,  $n = 18$ ). By comparing the  
301 frequency in SE and NE skin samples, we identified six mutations significantly enriched in SE  
302 samples: *TP53* R248W, *NOTCH1* P460L, *NOTCH1* S385F, *NOTCH1* E424K, *TP53* G245D and  
303 *NOTCH1* P460S, and nearly all of them were exclusively found in SE samples (FDR  $p < 0.05$ ,  
304 **Figure 2b**). No mutation was significantly enriched in NE samples. Five of the six SE-enriched  
305 mutations were found in both discovery and validation cohorts, suggesting they were unlikely to  
306 be caused by batch-effect. Unexpectedly, one specific mutation (*NOTCH1* E424K) was  
307 associated with significantly elevated VAFs (median = 10%,  $p < 0.001$ , Wilcoxon test), about five-  
308 fold higher than other mutations (median VAF = 2.1%, **Figure 2a, 2b**). Through protein structure  
309 modelling (**Figure 2c**), we found that the *NOTCH1* E424K mutation is predicted to disrupt the  
310 binding of *NOTCH1* to delta-like canonical ligand 4 (*DLL4*), a negative regulator of the Notch  
311 signaling pathway<sup>11</sup>. By prohibiting formation of a salt bridge between *NOTCH1* E424 and *DLL4*  
312 K189/R191, the mutation E424K creates a repulsive force that inhibits *DLL4* binding<sup>24</sup>. Based on  
313 the biological role of *DLL4* and *NOTCH1*, the *NOTCH1* E424 mutation is expected promote  
314 epithelial proliferation<sup>25,26</sup>. The overall prevalence of the *NOTCH1* E424K mutation in our dataset  
315 is 2.7%. For comparison, in GENIE cBioPortal<sup>27</sup>, *NOTCH1* E424K is mutated in 1.3% of  
316 cutaneous SCCs, 0.04% in melanomas, and is rarer in other cutaneous or non-cutaneous  
317 malignancies (**Table S5**).

318

### 319 **UV-signature mutations exclusively account for the elevated mutation burdens in SE skin**

320 We next intercorrelated the identified mutations with previously known UV-signature mutations  
321 (USMs), i.e., C>T transition at dipyrimidines<sup>4</sup>. Among all 638 mutations in SE and NE samples,

322 298 were USMs. Of these 298 USMs, 76% were present in SE samples. USMs were significantly  
323 enriched in SE compared to NE samples ( $n = 226$  and  $72$ , respectively,  $p < 0.001$ , Fisher's exact  
324 test). Especially among the high-VAF mutations, 18 of 19 mutations with VAFs above 0.1 were  
325 from SE samples, and most (13 of 18) were USMs. Conversely, non-UV-signature mutations  
326 (NUSMs) were present approximately equally ( $n = 159$  and  $181$ , ns, Fisher's exact test) in SE and  
327 NE skin types (**Figure 3a**), suggesting these mutations were not directly associated with UV-  
328 exposure.

329 To explore specific community enrichment patterns in different mutational function groups, we  
330 classified all 638 mutations into four effect-groups: nonsense, missense, silent and noncoding.  
331 Inside each effect-group, we correlated the mutational properties (USM vs NUSM) with the  
332 matched samples' sun-exposure statuses (SE vs NE) (**Figure 3b**). Significant enrichment of  
333 USMs were observed in two of four effect-groups by Fisher's exact test: nonsense (FDR  $p < 0.05$ )  
334 and missense (FDR  $p < 0.001$ ). Specifically, nonsense mutations were 9 times more frequently  
335 occurring in SE skins than in NE skins, and similarly enriched by 4.2 times for missense mutations.  
336 These findings strongly suggest the mutations initiated by UV radiation are further selected by the  
337 host system or inter-clonal competition<sup>28</sup>, in which the mutations with functional impacts give the  
338 host clone greater fitness.

339

#### 340 **Quantification of UV-induced DNA damage level by UV-signature mutations**

341 We next investigated the feasibility of using CMs to quantify UV-induced DNA damage. This was  
342 based on the hypothesis that SE samples harbor more CMs and are associated with higher VAFs  
343 compared to NE samples. Since our analyses indicated NUSMs were not correlated with UV  
344 exposure, only USMs were used for quantifying UV-induced DNA damage. To avoid the potential  
345 bias introduced by different punch sizes, only the most abundant size of 2 mm ( $n = 90$  and  $89$ ,

346 SE and NE, respectively) (**Figure 3c**) was analyzed. A three-fold difference was observed in the  
347 average USMs per sample between SE (mean = 1.2) and NE (mean = 0.4), which was  
348 significantly higher ( $p < 0.001$ , Wilcoxon test). Multiple USMs were found in 33% of SE samples  
349 but only 9% of NE samples (**Table S6**). Additionally, the identified USMs had significantly higher  
350 VAFs in SE (mean = 3.7%) than NE (mean = 2.1%) samples, ( $p < 0.001$ , Wilcoxon test),  
351 suggesting the presence of larger clones in SE samples (**Figure 3d**). We further extended the  
352 analysis to include all punch sizes, and found the pattern was consistent with 34% of SE and only  
353 6% of NE samples having multiple USMs and three-fold higher average USMs per sample in SE  
354 (1.0) than NE (0.3) samples ( $p < 0.001$ , Wilcoxon test).

355 In order to overcome the heterogeneity between samples, we developed Cumulative Relative  
356 Clonal Area (CRCA) as a single metric to assess the overall patient-level burden of CMs. The  
357 CRCA was defined as the overall percentage of biopsied skin area covered by USMs in a patient  
358 skin punch, which account for both the number of USMs and their VAFs (**Figure 3e**). It is worth  
359 mentioning that our data did not allow us to distinguish whether mutations occurred independently  
360 or were present in the same clone. Hence, CRCA does not provide an exact measure of the  
361 mutated cell population, but rather serves as an index of the mutation burden in the sampled area.  
362 To minimize the potential chance for repeated counting of co-occurring mutations in the same  
363 cells, co-occurring mutations were identified, primarily dinucleotide CC>TT mutations, and  
364 consolidated. When counted separately by sun-exposure status, the median CRCA across the 13  
365 patients was 6.1% (range 1.4-14.2%) in SE and 1.4% (range 0.1-4.0%) in NE sites. On individual  
366 patient level, the CRCAs were higher in SE than the matched NE skin in all patients, with the  
367 average ratio of 11.2-fold higher (range = 1.4 - 55.0-fold). These CRCAs were calculated using  
368 only USMs. If all CMs were included, the CRCA would be only 2.2-fold higher (range = 0.8 - 5.6-  
369 fold) in SE than NE skin (data not shown).

370



### 371 **The effect of punch size on USM detection**

372 In the discovery cohort, we sought to evaluate different punch sizes to determine the most efficient  
373 one for detecting USMs. Theoretically, although larger punches likely contain more clones, they  
374 tend to become less effective for detecting smaller clones due to a dilutional effect by other clones  
375 harboring no or different mutations (**Figure 4a**). Overall across all five punch sizes, USMs were  
376 detected in 54% of the SE, which was significantly higher than the 21% of the NE ( $p < 0.001$ ,  
377 Fisher's exact test). Between different punch sizes, 2 mm punches were found to have the highest  
378 positive rate of 64%, and with the most significant difference between SE and NE samples ( $p <$   
379  $0.0001$ , **Figure 4b**). Thus, only 2mm punches were collected in the 90-sample validation cohort  
380 and the extended cohort from cSCC patients. In the validation cohort, similarly, we found the SE  
381 samples had higher numbers of USMs and the positive rate of USMs (69%) was similar to the  
382 discovery cohort (64%).

383 When combining the discovery and validation cohorts, the SE samples had the highest positive  
384 rate of 67% for USMs in 2 mm samples and were significantly higher than NE samples ( $p < 0.001$ ),  
385 followed by 60% in 4 mm ( $p < 0.05$ ), and 54% in 3 mm ( $p < 0.05$ ). Interestingly, the USM positive  
386 rates were relatively lower in the largest punch size of 6 mm (53%) and the smallest 1 mm (36%).  
387 In all NE samples, positive USM rates ranged from 17-30% (**Figure 4c**). Moreover, the punch  
388 size also affected the detected VAFs of the mutations. Specifically, in SE samples, larger punches  
389 were associated with smaller VAFs. The VAFs' standard deviation was the highest in 1 mm  
390 punches (8.9%) and decreased with punch size: 2 mm (4.3%), 3 mm (2.8%), 4 mm (2.6%) and 6  
391 mm (1.7%). This trend, between VAF range and punch size, was not present in NE samples  
392 (**Figure 4d**). Under the current condition, 2 mm was the most effective punch size in detecting  
393 USMs.

### 394 **Mutation nucleotide contexts enriched with UV-exposure**



395 We next assessed the enrichment of different mutation nucleotide contexts in SE skin. The  
396 mutation nucleotide contexts were defined by each SNV's trinucleotide and DNV's dinucleotide  
397 contexts. A total of 83 contexts were identified from current mutations, including 13 contexts  
398 matching to previously described USMs<sup>4</sup>. None of the remaining 70 non-USM contexts were  
399 enriched in SE or NE samples (**Figure 5a**). The 13 previously defined USM contexts were not  
400 equally enriched in SE samples. After multiple test correction, only 5 of the 13 contexts were  
401 significantly enriched in SE samples (FDR  $p < 0.05$ ), including the dinucleotide CC>TT context,  
402 which was exclusively found in SE samples (**Figure 5b**). The most significant mutation context  
403 enriched in SE samples was T[C>T]C (FDR  $p = 0.00013$ ), which was in consonance with the  
404 previously defined "Mutational Signature #7" in skin cancers<sup>29</sup>. The remaining eight UV-signature  
405 contexts were not significantly enriched in SE samples. Of particular note, G[C>T]C, which was  
406 the most abundant context by total number of mutations, appeared to be equally presented in SE  
407 and NE skin samples and therefore not associated with sun-exposure.

#### 408 **Clonal mutations are correlated with cSCC burden**

409 To define the clinical significance of CMs and investigate the potential association with skin cancer  
410 risk, we sequenced an extended cohort of 20 samples (16 SE normal skin and 4 cSCC) from eight  
411 patients with cSCC using a 59.5 kb customized panel as described above. Four individuals  
412 (including 8 normal skin samples and 2 cSCC samples from face, scalp, and arm) had a low  
413 burden of skin cancer with only a single diagnosis of cSCC and few AKs (low-cSCC). Four  
414 individuals (including 8 normal skin samples and 2 cSCC samples from face, hand, and lower leg)  
415 had a high burden of skin cancer with severe UV damage, multiple prior cSCC (range 3-10) and  
416 many AKs (high-cSCC). Normal skin samples were all sun-exposed, and were obtained a linear  
417 distance of either 1mm or 6mm from the clear surgical margin of the excised cSCC, allowing for  
418 analysis of CMs arising in skin subjected to carcinogenic UV radiation. Visible AKs were not  
419 present in normal skin samples. A total of 535 somatic mutations were identified (**Table S7**), with

420 a median VAF of 1.2%. Only 15 mutations had VAF greater than 10%, most of which (10 of 15)  
421 were from the cSCC tumor samples (**Figure 6a**). The median numbers of mutations per sample  
422 in each group were 22 and 17.5 for the high- and low- cSCC normal skin samples (marginally  
423 significant,  $p=0.078$ , Wilcoxon), and 41.5 for the cSCC samples. The overall mutation rates in  
424 normal skin were 0.45 and 0.29 mutations per MB, in high- and low-cSCC patients, respectively.  
425 The latter was comparable to the rate of SE normal skin of non-cancer patients in the primary  
426 cohort (0.31 mutations per MB), despite the technical differences between the two cohorts such  
427 as sequencing depth, targeted regions and punch sizes.

428 The frequently mutated genes in the normal skin (more than two mutations per gene on  
429 average) included *FAT1*, *NOTCH1*, *NOTCH2*, *NOTCH3*, *FGFR3* and *TP53* (**Figure 6b**). Two of  
430 the genes were mutated at least twice as frequently in the normal skin of high-cSCC patients as  
431 that of low-cSCC patients: *TP53* (high-cSCC/Low-cSCC ratio = 3.25) and *FAT1* (ratio = 2.4).  
432 Additionally, two less frequently mutated genes, *KRAS* and *HRAS*, were almost exclusively  
433 mutated in high-cSCC patients (9 of 10). None of these differences reached statistical significance  
434 after multiple test correction (data not shown), suggesting larger cohorts will be needed to further  
435 explore these potential associations.

436 Although the normal skin of high-cSCC patients contain more mutations per sample,  
437 unexpectedly, these mutations were associated with significantly lower VAFs (median=1.0%) than  
438 the normal skin of low-cSCC patients (median = 1.3%,  $p = 0.011$ , Wilcoxon). We found this overall  
439 reduction in VAF resulted from a higher number of low-frequency mutations in high-cSCC patients  
440 (**Figure 6c**). For mutations with VAF greater than 1%, the mutations were equally present in high-  
441 and low-cSCC patients. However, for low-VAF mutations (defined as <1%), the numbers of  
442 mutations per sample were significantly higher in high-cSCC (median = 9.5) than low-cSCC  
443 patients (median = 6,  $p = 0.032$ , Wilcoxon, **Figure 6d**).

444 We next further refined the analysis by focusing on USMs. There were a total of 206 USMs,  
445 including 8 CC>TT DNVs. We observed a significantly greater number of USMs in the high-cSCC  
446 normal skin samples (median = 11) than the low-cSCC ones (median = 6.5, FDR  $p = 0.015$ )  
447 **(Figure 6e)**. The tumor samples were found to harbor even higher numbers of USMs (median =  
448 15.5). The CRCA values, as defined in the primary cohort, were significantly higher in the tumor  
449 than the normal skin samples (FDR  $p = 0.03$ ) in the extended cohort. The normal skin samples  
450 from high-cSCC patients had slightly higher CRCAs (median = 0.37) than the ones from low-  
451 cSCC patients (median = 0.31), but the difference was not statistically significant ( $p = 0.16$ ). The  
452 lack of significance is likely due to the majority of the difference between high-cSCC and low-  
453 cSCC normal skin samples is due to mutations with VAFs below 1%. Focusing on only low-  
454 frequency mutations (VAF < 1%), the CRCA values were significantly higher in normal skin of  
455 high-cSCC patients than the low-cSCC patients ( $p = 0.014$ , **Table S8**). These findings indicate  
456 that CRCA is a sensitive measure of UV-induced DNA damage, but may be further refined by  
457 focusing on low-frequency mutations to assess cSCC risk. Further, no significant difference was  
458 found between normal skin samples collected at 1mm and 6mm from the surgical margin, by the  
459 overall mutation burden, VAF, or USMs. Lastly, almost all mutations (>99%) were only in one but  
460 not in other samples of the same patient. The absence of shared recurrent mutations across  
461 different samples from the same individual suggested that the identified mutations arose  
462 independently.

## 463 **Discussion**

464 Most cancers are initiated by accumulation of somatic mutations<sup>30,31</sup>. However, early mutations in  
465 normal tissues are difficult to detect due to the low relative abundance and random patterns.  
466 Several recent studies demonstrated the feasibility of detecting clonal mutations (CMs) using  
467 high-throughput sequencing in various tissue types<sup>11,12,32</sup>. However, the contribution of these CMs

468 to cancer remains unclear in several important areas: how they are generated, what types of  
469 mutations are generated by which exogenous and endogenous carcinogens; how the CMs are  
470 accumulated and selected by the host microenvironment and inter-clonal competition <sup>28</sup>; and  
471 which mutations contribute or lead to the development of cancer. Indeed, all types of tissues are  
472 under the influence of multiple intrinsic and extrinsic factors that vary greatly by individual's  
473 lifestyle and environment. Therefore, studying the CMs generated by one specific carcinogen  
474 requires comparative studies of matched sample types.

475 To the best of our knowledge, the current study of paired SE and NE skin areas is the first  
476 comprehensive analysis of individual-matched normal human skin to specifically characterize UV  
477 radiation's mutational effects. We optimized our approach for detecting UV-induced CMs by: 1)  
478 acquiring matched SE/NE skin samples from the same individual to control for aging and other  
479 environmental factors unrelated to UV; 2) separating epidermal from dermal layers decreases  
480 non-epidermal background DNA quantity; 3) ultra-deep DNA sequencing for maximized sensitivity,  
481 followed by error-suppression to exclude sequencing and alignment errors. Consistent with  
482 previous studies <sup>11,12</sup>, CMs were widespread in epidermal samples. As expected, mutation burden  
483 and VAFs were significantly elevated in SE samples. The mutational signatures of the current  
484 CMs are consistent with those previously found in skin cancers <sup>29</sup>, supporting the contribution of  
485 the CMs to potential ongoing tumorigenesis. Markedly, our unique approach allowed us to identify  
486 several important new insights about epidermal CMs. First, we identified the existence of  
487 "mutation-exempt" regions in human genomes. Although mutations frequently occur across most  
488 of the sequenced regions in NE skin, presumably due to metabolism and aging related factors,  
489 no detectable mutations were found in these mutation-exempt regions. It is unclear whether the  
490 absence of mutations in these genomic regions is caused by an active protection or a passive  
491 selection mechanism involving altered clone fitness. Interestingly, the "mutation-exempt" property  
492 of these regions appears to be altered upon exposure to UV radiation, and these regions become

493 highly mutable. Further studies are warranted to explore how this mechanism is abrogated by UV  
494 radiation. Second, USMs were significantly enriched in Glutamate Metabotropic Receptor 3  
495 (*GRM3*) in SE skin, which was previously identified as a potential therapeutic target in melanoma  
496 <sup>33</sup>, but not reported as a cancer driver in cutaneous SCC. Third, we identified six mutations that  
497 were almost exclusively mutated in SE skin. All six mutations had been previously reported in  
498 human cutaneous squamous cell carcinomas in the cBioPortal <sup>27</sup>. Among these mutations, *TP53*  
499 R248W and G245D were highly recurrent with hundreds of occurrences reported in *COSMIC* <sup>34</sup>,  
500 suggesting that the presence of these mutations may be representative of an early phase of  
501 carcinogenesis.

502 Consistent with the current finding that UV-exposure results in higher USM burden, and the  
503 known knowledge that UV-exposure directly correlates with the risk of cSCC <sup>35</sup>, the results of our  
504 extended cohort of cSCC patients provided direct evidence that elevated USM burdens are  
505 associated with increased cSCC risk. Unexpectedly, we further discovered that most mutational  
506 difference between normal skin of high- and low-cSCC patients derived from low frequency clones  
507 (VAF<1%) but not the “expanded” clones (VAF≥1%). It remains unclear why such difference was  
508 not seen in the expanded clones. One potential explanation is that the expanded clones might be  
509 under more aggressive immune surveillance, as it has been previously reported that the immune  
510 system preferably targets larger clones than smaller ones <sup>36</sup>. The low frequency clones, on the  
511 other hand, are less actively monitored by the immune system and may more truthfully represent  
512 the level of ongoing mutational activity.

513 Our approach was directed by future clinical utilities, focusing on quantitative measurement of  
514 UV-induced DNA damage for sun-protection, and cSCC patient risk stratification. These results  
515 demonstrate the feasibility of using a small panel of genomic regions (5.5 kb) to quantitatively  
516 measure UV-induced CMs. We established Relative Cumulative Clonal Area (CRCA) as a  
517 combined measure of mutation burden and relative abundance, which showed an overall 11.2-

518 fold difference between patient-matched SE/NE samples. In the current study, we found the most  
519 effective punch size for capturing CMs was 2 mm, which is also clinically favorable as it leaves  
520 relatively smaller scars due to the small diameter punch. In future, a non-invasive skin sampling  
521 method may provide even wider accessibility to epidermal sampling. In addition, the efficiency of  
522 this panel is related to the performance of sequencing method and mutation calling algorithm,  
523 which will likely be improved with adoption of more sensitive future methods focusing on the  
524 genomic hotspots that are sensitive to UV exposure.

525 The current study focused on the most frequently mutated regions in sun-exposed skin  
526 samples defined by the mutations in a previous study <sup>12</sup>. However, we note that many of these  
527 regions are mutated in both sun-exposed and non-sun-exposed skin samples, suggesting many  
528 mutations in these regions were unrelated to UV exposure. In fact, only 6 of 55 original regions  
529 were found to harbor significantly enriched mutations in SE samples. Future studies, including  
530 much larger targeted regions, are needed to systematically identify UV-sensitive genomic regions.  
531 The skin samples were collected at the same time; therefore, they do not provide longitudinal  
532 information about clone initiation and progression. While our analyses of the extended cohort  
533 suggest the burdens of CMs in normal skin are correlated with cancer risk in cSCC patients, this  
534 finding needs to be validated in a larger cohort of patients. Future studies including biopsies of  
535 both SCC and adjacent normal skin acquired at multiple time points are warranted to unveil the  
536 complete role of these CMs in cancer.

537

## 538 **Conclusions**

539 In summary, this study revealed previously unknown mutational patterns associated with UV-  
540 exposure, providing important insights into UV radiation's early carcinogenic effects. The  
541 quantification of CMs has the potential to become the cornerstones for future development of

542 quantitative measures of UV-induced DNA damage, as measured by CRCA, in the clinical setting  
543 to monitor early carcinogenesis and highlight the importance of sun protection. The identified  
544 association between cSCC risk and the burdens of CMs, especially low-frequency CMs, if  
545 validated in an expanded cohort, may become a novel biomarker for risk stratification of cSCCs.

546

#### 547 **List of abbreviations**

#### 548 **Ethics Statements**

549 All specimens were collected from post-mortem donors collected in collaboration with Buffalo's  
550 local organ procurement organization (ConnectLife, formerly Unyts) the Roswell Park's Rapid  
551 Tissue Acquisition Program under a Roswell Park approved IRB protocol.

#### 552 **Availability of data and materials**

553 The datasets used and/or analyzed during the current study are available from the  
554 corresponding authors upon request.

#### 555 **Competing interests**

556 None.

#### 557 **Funding**

558 This work was mainly supported by the Roswell Park Alliance Foundation. LW and SL were  
559 supported in part by NIH grant U24CA232979. The utilized Genomics and Bioinformatics Shared  
560 Resources and Rapid Tissue Acquisition Program at Roswell Park Comprehensive Cancer

561 Center was supported by NCI grant P30CA016056. LW and JX were supported in part by a travel  
562 grant from NIH 5U24ES026465.

### 563 **Acknowledgments**

564 The authors thank the excellent technical help provided by Paula Pera, MS.

### 565 **Common Abbreviations:**

566 UV – Ultraviolet

567 CM – Clonogenic mutation

568 NMSC – Nonmelanoma skin cancer

569 SE – Sun-exposed

570 NE – Non-sun-exposed

571 USM – UV-signature mutation

572 NUSM – Non-UV-signature mutation

573 CRCA – Cumulative Relative Clonal Area

574 cSCC – Cutaneous squamous cell carcinoma

575 AK – Actinic keratosis

576 SNV – Single nucleotide variant

577 Indels – Insertions/deletions

578 DNV – Dinucleotide variant

579 CSNV – Cluster of single nucleotide variant

580 MAC – Multi-Nucleotide Variant Annotation Corrector

581 VAF – Variant allele frequency



582 **Figure Legends**

583 **Figure 1. Region-specific enrichment of somatic mutations in sun-exposed skin.** a). Graph  
584 shows the number of mutations identified within each 100-bp genomic target window grouped by  
585 SE and NE skin types. b). The overall gene-level percentage of mutations from SE and NE  
586 samples. Stars indicate the segments or genes where mutations are significantly enriched in the  
587 SE samples (FDR p values: \*\*\*  $p < 0.001$ ; +  $p < 0.1$ ).

588 **Figure 2. Hotspots and mutations associated with UV-exposure.** a). All mutations are ordered  
589 by their genomic locations. X-axis: the order of the mutation's genomic location. Y-axis: variant  
590 allele fraction (VAF) of individual mutations. Color depicts the gene harboring the mutations. The  
591 three genes demonstrating significant difference between SE and NE, either on the gene level or  
592 segment level, were labeled on top (*TP53*, *GRM3*, *NOTCH1*). One specific mutation with elevated  
593 VAFs (*NOTCH1* E424K) is indicated with a red arrow. b). The VAF of the six individual mutations  
594 that are significantly enriched in SE vs NE epidermis in the primary discovery (green) and  
595 validation (brown) data sets. The dotted red line represents median VAF of all mutations and  
596 black lines indicate the median of each group. c). The predicted protein complex structure of  
597 *NOTCH1* and *DLL4* to show the position of the mutant E424K and the interacting partners, *DLL4*  
598 K189/R191, in wild type.

599 **Figure 3. UV-induced DNA damage assessed by USMs.** a). Only UV-signature mutations are  
600 associated with sun-exposure status. Left: higher numbers of USMs are found in SE than NE skin.  
601 Right: NUSMs are almost equally presented in SE and NE samples. Red dotted line indicates  
602 high-VAF ( $> 0.1$ ). Black dotted circle indicates extra USMs in SE skin compared with NE skin. b).  
603 The numbers of mutations by each amino-acid-change type found in SE and NE skin, grouped  
604 by USMs and NUSMs. Overall distribution c.) of the numbers of USMs per sample and d.) the  
605 VAFs of the mutations using the 2 mm punch size. Inside the violin plots: black dots - original

606 data points from individual samples; yellow dot with bar - averaged value with standard deviation.  
607 SE samples are associated with higher numbers of USMs, as well as higher VAFs indicating  
608 potential larger clones. **e**). Cumulative Relative Clonal Area (CRCA) was developed to represent  
609 the overall percentage of the biopsied skin areas that are covered by clonal mutations. In all 13  
610 current individuals, CRCAs were higher in SE than in the matched NE group, with the ratios of  
611 SE/NE ranged from 1.4 to 55.0 (mean = 11.2). Statistical tests used: figure 3b, Fisher's exact test  
612 with multiple test correction implemented using the FDR method; figure 3c, 3d: Wilcoxon test;  
613 \* $p < 0.05$ , \*\* $p < 0.01$ , \*\*\* $p < 0.001$ .

614 **Figure 4. Optimization of punch size for detecting USMs.** a). A representative figure showing  
615 one representative punch of each collection size. We selected the sample with the highest number  
616 of mutations under each size for easy illustration. Every mutation is plotted as a dot with its size  
617 calculated to match the clonal area harboring the mutation. One punch size, 3 mm was not shown  
618 as it was obtained by cutting a 6 mm punch into quarters. b). In the discovery cohort, 2 mm was  
619 found to be the most efficient size in differentiating CRCA from SE and NE skin samples by p  
620 value. c). Distribution of numbers of USMs per sample at each punch size, after combining both  
621 the discovery and validation cohorts. d). VAF of USM detected in different size punches. The size  
622 of the dot indicates the approximate relative area of cells containing the mutation. In SE samples,  
623 VAFs of USMs detected from larger punches are associated with smaller variations.

624 **Figure 5. Mutational contexts associated with UV-exposure.** a). Each dot represents a specific  
625 mutation context of SNVs and DNVs. X-axis: the total numbers of mutations of each context; y-  
626 axis: p value of the context for differentiating SE and NE skin, shown as  $-\log(p)$ . The dotted line  
627 indicate  $p < 0.05$  (the above area). None of the NUSM contexts was significant. b). Further  
628 refinement of USM contexts by depicting the numbers of mutations in SE and NE skin for all  
629 current USM contexts. Mutation contexts are ordered by the p value of SE vs NE in an increasing

630 order from left to right. Multiple test correction was implemented using the FDR method. The  
631 dotted line indicates FDR  $p < 0.05$  (the left side).

632

633 **Figure 6. Clonal mutations are correlated with cSCC burden.** a). Violin plots depicting the  
634 overall distribution of somatic mutations in each sample. Ordered by sample type, and then by  
635 the distance from the surgical margin. b). Mutation numbers by genes in the normal skin. NS (high)  
636 - normal skin from high-cSCC patients; NS(low) - normal skin from low-cSCC patients. c). High-  
637 cSCC patients are associated with increased low-*VAF* (<1%) mutations. Histogram depicting the  
638 distribution of *VAFs* of the detected mutations in normal skin separated by patient risk. The dotted  
639 oval highlights the increased low-*VAF* mutations in the normal skin of high-cSCC patients  
640 compared with low-cSCC patients. d) Number of mutations per sample in normal skin, separated  
641 by high- ( $\geq 1\%$ ) and low- (<1%) *VAFs*; e) Number of USMs per sample in high- and low- cSCC  
642 normal skin (NS), and cSCC tumors. Shape indicates the two normal skin samples from each  
643 patient, taken from either 1mm (circle) or 6mm (triangle) sample at the surgical margin.

644 **Tables**

645 Table 1. Patient and sample cohort

Patient	Control (dermis)	Epidermis SE/NE pairs						Total SE/NE pairs
		1 mm	2 mm	3 mm*	4 mm	6 mm	2 mm <sup>#</sup>	
Pt1	1		5	4	1	1		11
Pt2	1	3	5	4	1	1		14
Pt3	1	3	5	4	1	1		14
Pt4	1	3	3					6
Pt5	1	3	3	3	3	3	5	20
Pt6	1	3	3	3	3	3	5	20
Pt7	1	3	3	3	3	3	5	20
Pt8	1	3	3	3	3	3	5	20
Pt9	1	3	3	3	3	3	5	20
Pt10	1	3	3	3	3	3	5	20
Pt11	1	3	3	3	3	3	5	20
Pt12	1	3	3	3	3	3	5	20
Pt13	2	3	3	3	3	3	5	20
Total	14	36	45	39	30	30	45	225

646 \* 3 mm punches were obtained by cutting 6 mm punches into quarters

647 # Validation cohort containing only 2 mm punches

648

649 **References**

- 650 1 Rogers, H. W., Weinstock, M. A., Feldman, S. R. & Coldiron, B. M. Incidence Estimate of  
651 Nonmelanoma Skin Cancer (Keratinocyte Carcinomas) in the U.S. Population, 2012.  
652 *JAMA Dermatol* **151**, 1081-1086, doi:10.1001/jamadermatol.2015.1187 (2015).
- 653 2 Koh, H. K., Geller, A. C., Miller, D. R., Grossbart, T. A. & Lew, R. A. Prevention and early  
654 detection strategies for melanoma and skin cancer. Current status. *Arch Dermatol* **132**,  
655 436-443 (1996).
- 656 3 Marteijn, J. A., Lans, H., Vermeulen, W. & Hoeijmakers, J. H. Understanding nucleotide  
657 excision repair and its roles in cancer and ageing. *Nature reviews. Molecular cell biology*  
658 **15**, 465-481, doi:10.1038/nrm3822 (2014).
- 659 4 Brash, D. E. UV signature mutations. *Photochem Photobiol* **91**, 15-26,  
660 doi:10.1111/php.12377 (2015).
- 661 5 Wikonkal, N. M. & Brash, D. E. Ultraviolet radiation induced signature mutations in  
662 photocarcinogenesis. *J Investig Dermatol Symp Proc* **4**, 6-10 (1999).
- 663 6 Marks, R., Rennie, G. & Selwood, T. S. Malignant transformation of solar keratoses to  
664 squamous cell carcinoma. *Lancet* **1**, 795-797, doi:10.1016/s0140-6736(88)91658-3  
665 (1988).
- 666 7 Ling, G. *et al.* Persistent p53 mutations in single cells from normal human skin. *Am J*  
667 *Pathol* **159**, 1247-1253, doi:10.1016/S0002-9440(10)62511-4 (2001).
- 668 8 Brash, D. E. Cancer. Preprocancer. *Science* **348**, 867-868, doi:10.1126/science.aac4435  
669 (2015).
- 670 9 Urano, Y. *et al.* Frequent p53 accumulation in the chronically sun-exposed epidermis and  
671 clonal expansion of p53 mutant cells in the epidermis adjacent to basal cell carcinoma. *J*  
672 *Invest Dermatol* **104**, 928-932 (1995).
- 673 10 Williams, C. *et al.* Clones of normal keratinocytes and a variety of simultaneously present  
674 epidermal neoplastic lesions contain a multitude of p53 gene mutations in a xeroderma  
675 pigmentosum patient. *Cancer Res* **58**, 2449-2455 (1998).
- 676 11 Yizhak, K. *et al.* RNA sequence analysis reveals macroscopic somatic clonal expansion  
677 across normal tissues. *Science* **364**, doi:10.1126/science.aaw0726 (2019).
- 678 12 Martincorena, I. *et al.* Tumor evolution. High burden and pervasive positive selection of  
679 somatic mutations in normal human skin. *Science* **348**, 880-886,  
680 doi:10.1126/science.aaa6806 (2015).
- 681 13 Wei, L. *et al.* Accurate Quantification of Residual Cancer Cells in Pelvic Washing Reveals  
682 Association with Cancer Recurrence Following Robot-Assisted Radical Cystectomy. *J*  
683 *Urol* **201**, 1105-1114, doi:10.1097/JU.000000000000142 (2019).
- 684 14 Wei, L. *et al.* Pitfalls of improperly procured adjacent non-neoplastic tissue for somatic  
685 mutation analysis using next-generation sequencing. *BMC medical genomics* **9**, 64,  
686 doi:10.1186/s12920-016-0226-1 (2016).
- 687 15 Tang, J. *et al.* The genomic landscapes of individual melanocytes from human skin.  
688 *bioRxiv*, 2020.2003.2001.971820, doi:10.1101/2020.03.01.971820 (2020).

- 689 16 Huss, W. J. *et al.* Comparison of SureSelect and Nextera Exome Capture Performance in  
690 Single-Cell Sequencing. *Human heredity* **83**, 153-162, doi:10.1159/000490506 (2018).
- 691 17 Gamble, R. G. *et al.* Sun damage in ultraviolet photographs correlates with phenotypic  
692 melanoma risk factors in 12-year-old children. *J Am Acad Dermatol* **67**, 587-597,  
693 doi:10.1016/j.jaad.2011.11.922 (2012).
- 694 18 Creidi, P. *et al.* Profilometric evaluation of photodamage after topical retinaldehyde and  
695 retinoic acid treatment. *J Am Acad Dermatol* **39**, 960-965 (1998).
- 696 19 Li, H. & Durbin, R. Fast and accurate short read alignment with Burrows-Wheeler  
697 transform. *Bioinformatics* **25**, 1754-1760, doi:10.1093/bioinformatics/btp324 (2009).
- 698 20 Liu, Q. *et al.* SeqSQC: A Bioconductor Package for Evaluating the Sample Quality of Next-  
699 generation Sequencing Data. *Genomics Proteomics Bioinformatics* **17**, 211-218,  
700 doi:10.1016/j.gpb.2018.07.006 (2019).
- 701 21 Saunders, C. T. *et al.* Strelka: accurate somatic small-variant calling from sequenced  
702 tumor-normal sample pairs. *Bioinformatics* **28**, 1811-1817,  
703 doi:10.1093/bioinformatics/bts271 (2012).
- 704 22 Wei, L. *et al.* MAC: identifying and correcting annotation for multi-nucleotide variations.  
705 *BMC genomics* **16**, 569, doi:10.1186/s12864-015-1779-7 (2015).
- 706 23 Newman, A. M. *et al.* Integrated digital error suppression for improved detection of  
707 circulating tumor DNA. *Nat Biotechnol* **34**, 547-555, doi:10.1038/nbt.3520 (2016).
- 708 24 Luca, V. C. *et al.* Structural biology. Structural basis for Notch1 engagement of Delta-like  
709 4. *Science* **347**, 847-853, doi:10.1126/science.1261093 (2015).
- 710 25 Blanpain, C., Lowry, W. E., Pasolli, H. A. & Fuchs, E. Canonical notch signaling functions  
711 as a commitment switch in the epidermal lineage. *Genes Dev* **20**, 3022-3035,  
712 doi:10.1101/gad.1477606 (2006).
- 713 26 Lefort, K. & Dotto, G. P. Notch signaling in the integrated control of keratinocyte  
714 growth/differentiation and tumor suppression. *Semin Cancer Biol* **14**, 374-386,  
715 doi:10.1016/j.semcancer.2004.04.017 (2004).
- 716 27 Gao, J. *et al.* Integrative analysis of complex cancer genomics and clinical profiles using  
717 the cBioPortal. *Science signaling* **6**, pl1, doi:10.1126/scisignal.2004088 (2013).
- 718 28 Colom, B. *et al.* Spatial competition shapes the dynamic mutational landscape of normal  
719 esophageal epithelium. *Nat Genet*, doi:10.1038/s41588-020-0624-3 (2020).
- 720 29 Alexandrov, L. B. *et al.* Signatures of mutational processes in human cancer. *Nature* **500**,  
721 415-421, doi:10.1038/nature12477 (2013).
- 722 30 Wu, S., Powers, S., Zhu, W. & Hannun, Y. A. Substantial contribution of extrinsic risk  
723 factors to cancer development. *Nature* **529**, 43-47, doi:10.1038/nature16166 (2016).
- 724 31 Tomasetti, C. & Vogelstein, B. Cancer etiology. Variation in cancer risk among tissues can  
725 be explained by the number of stem cell divisions. *Science* **347**, 78-81,  
726 doi:10.1126/science.1260825 (2015).
- 727 32 Martincorena, I. *et al.* Somatic mutant clones colonize the human esophagus with age.  
728 *Science*, doi:10.1126/science.aau3879 (2018).
- 729 33 Kunz, M. The genetic basis of new treatment modalities in melanoma. *Curr Drug Targets*  
730 **16**, 233-248, doi:10.2174/1389450116666150204112138 (2015).

- 731 34 Forbes, S. A. *et al.* The Catalogue of Somatic Mutations in Cancer (COSMIC). *Curr Protoc*  
732 *Hum Genet* **Chapter 10**, Unit 10 11, doi:10.1002/0471142905.hg1011s57 (2008).
- 733 35 Johnson, T. M., Rowe, D. E., Nelson, B. R. & Swanson, N. A. Squamous cell carcinoma  
734 of the skin (excluding lip and oral mucosa). *J Am Acad Dermatol* **26**, 467-484,  
735 doi:10.1016/0190-9622(92)70074-p (1992).
- 736 36 Gejman, R. S. *et al.* Rejection of immunogenic tumor clones is limited by clonal fraction.  
737 *Elife* **7**, doi:10.7554/eLife.41090 (2018).
- 738

**Figure 1. Region-specific enrichment of somatic mutations in sun-exposed skin**

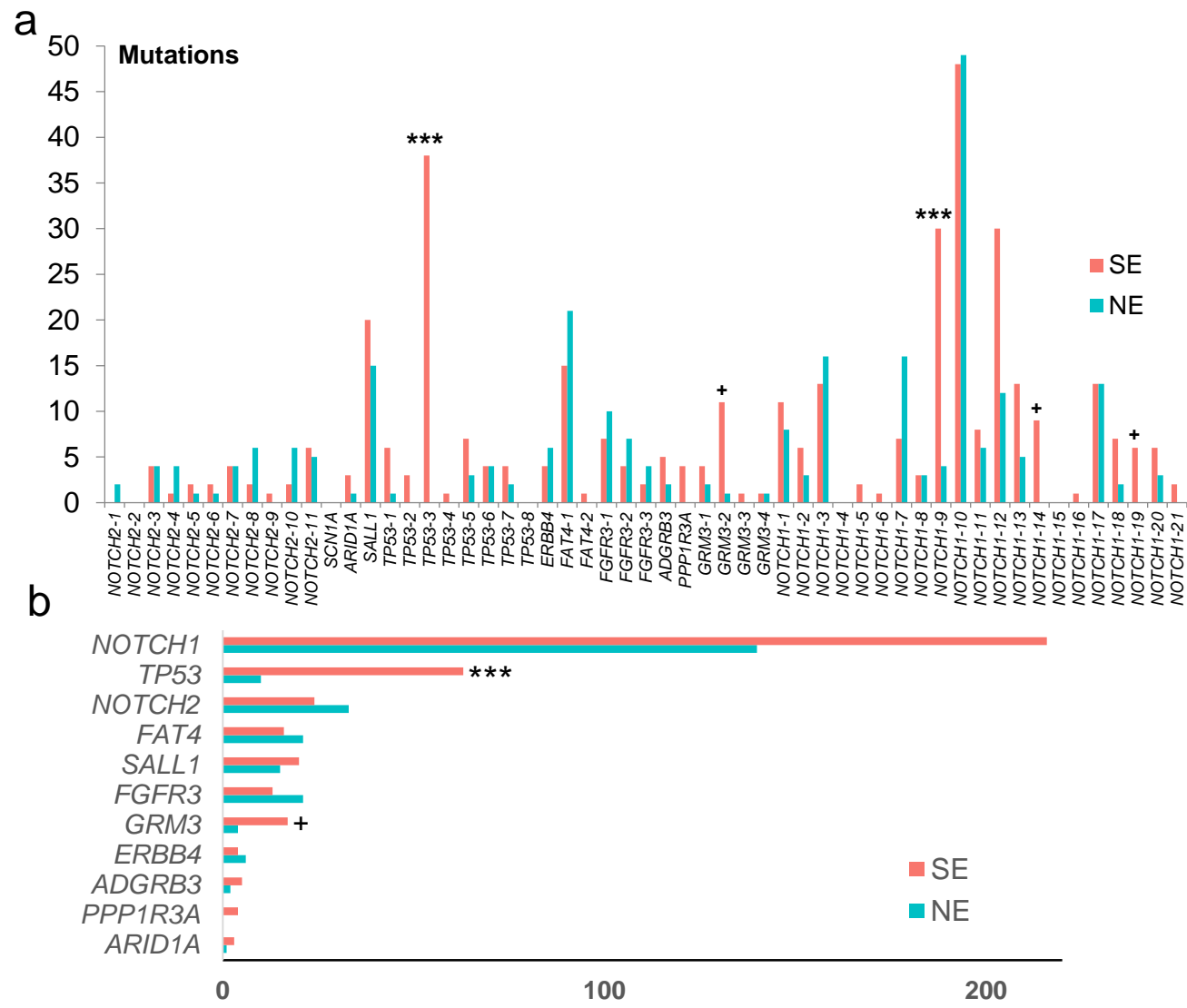
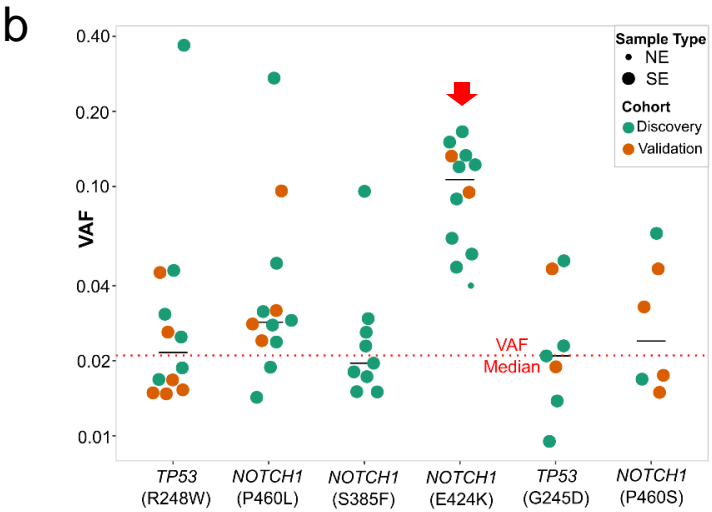
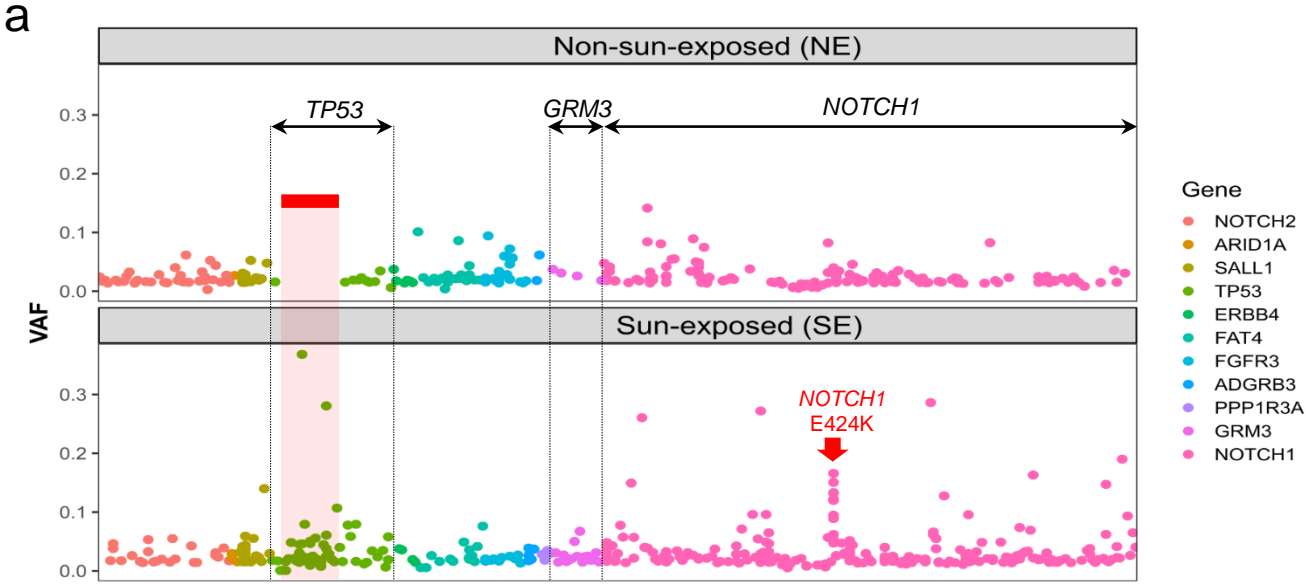




**Figure 2. Hotspots and mutations associated with UV-exposure.**



**c**

NOTCH1

EGF11<sup>424(K)</sup>

DSL

DLL4

**Figure 3. UV-induced DNA damage assessed by USMs**

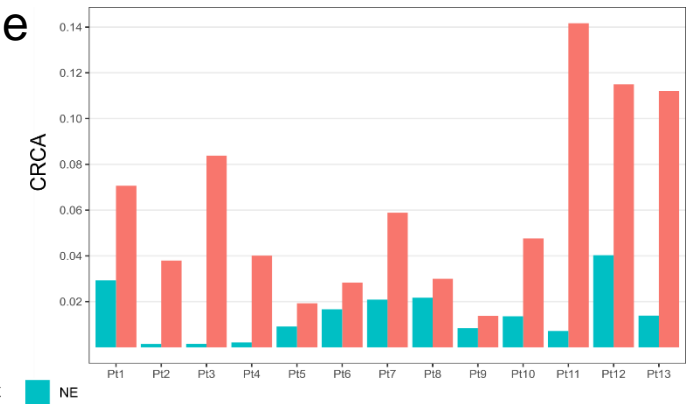
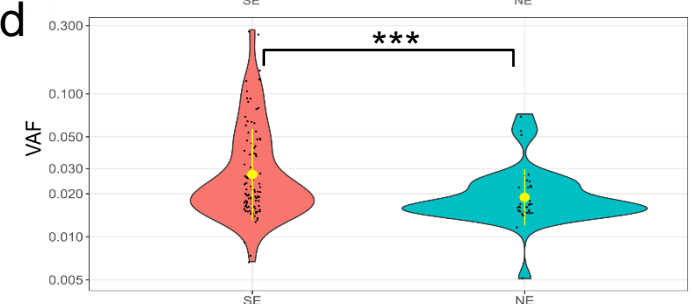
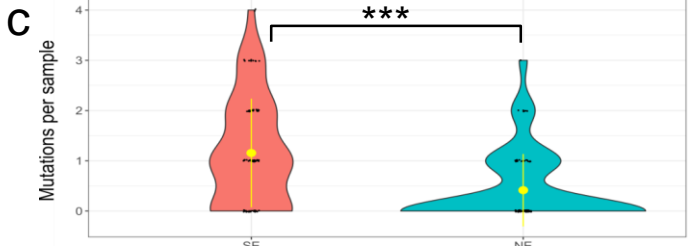
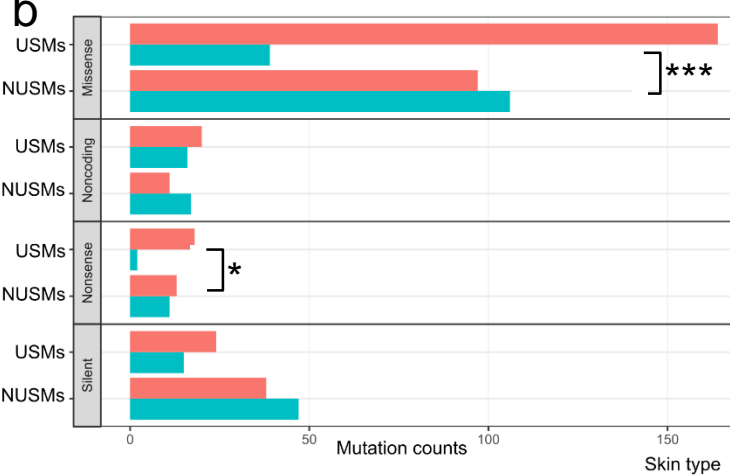
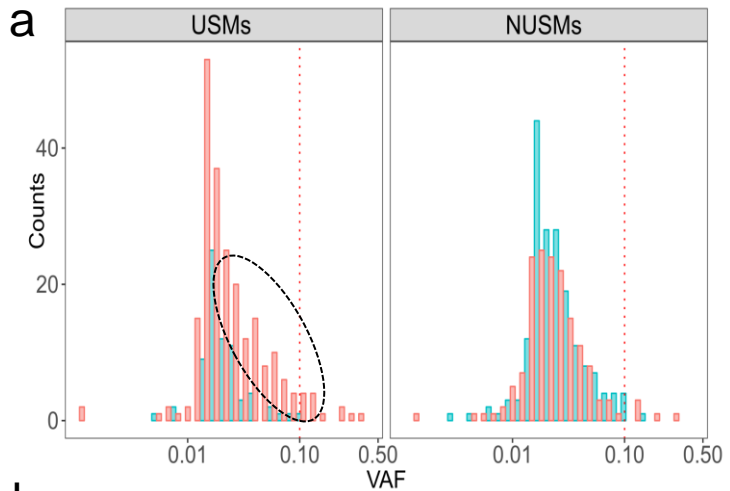


**Figure 4. Optimization of punch size for detecting USMs**

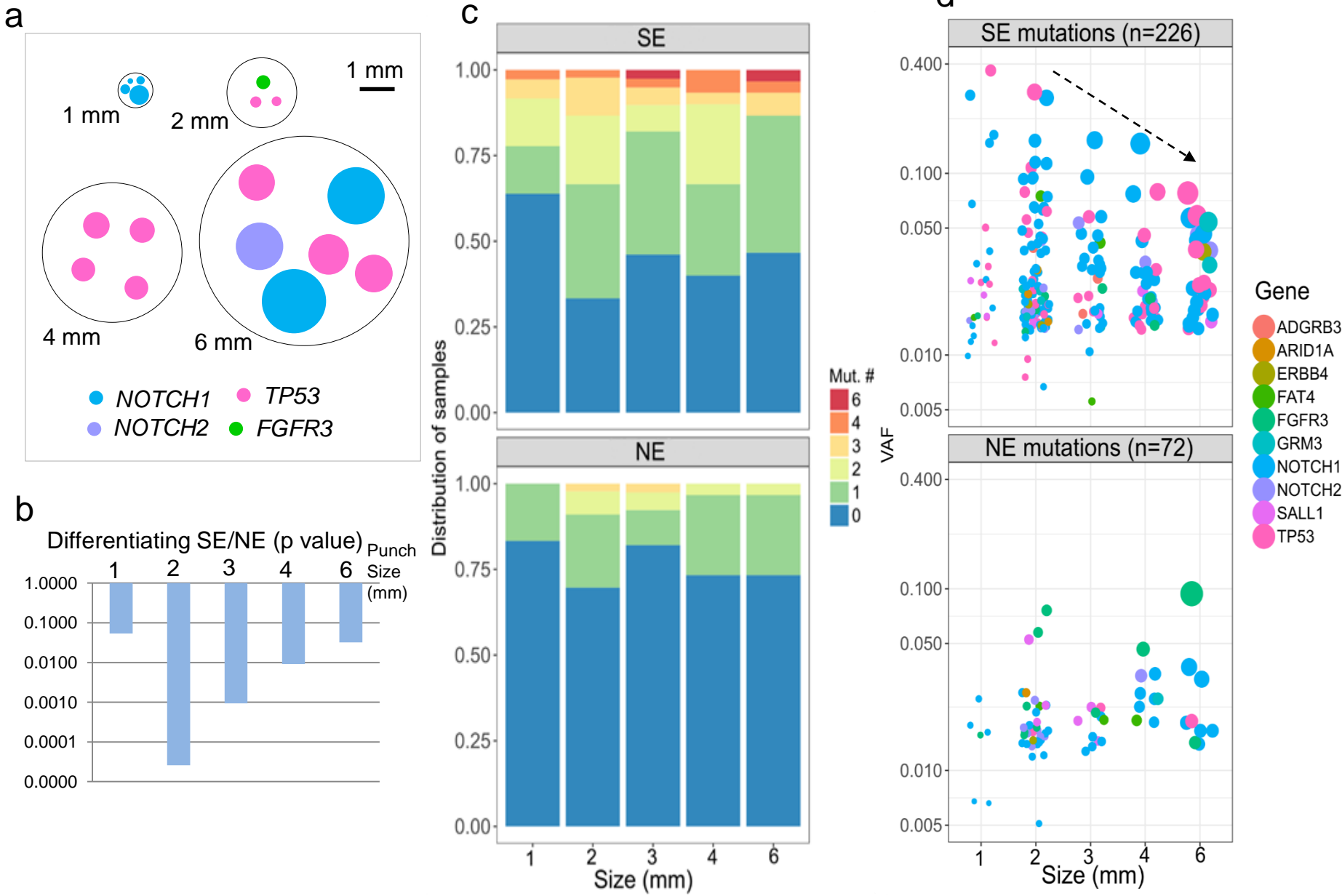


**Figure 5. Mutational contexts associated with UV-exposure**

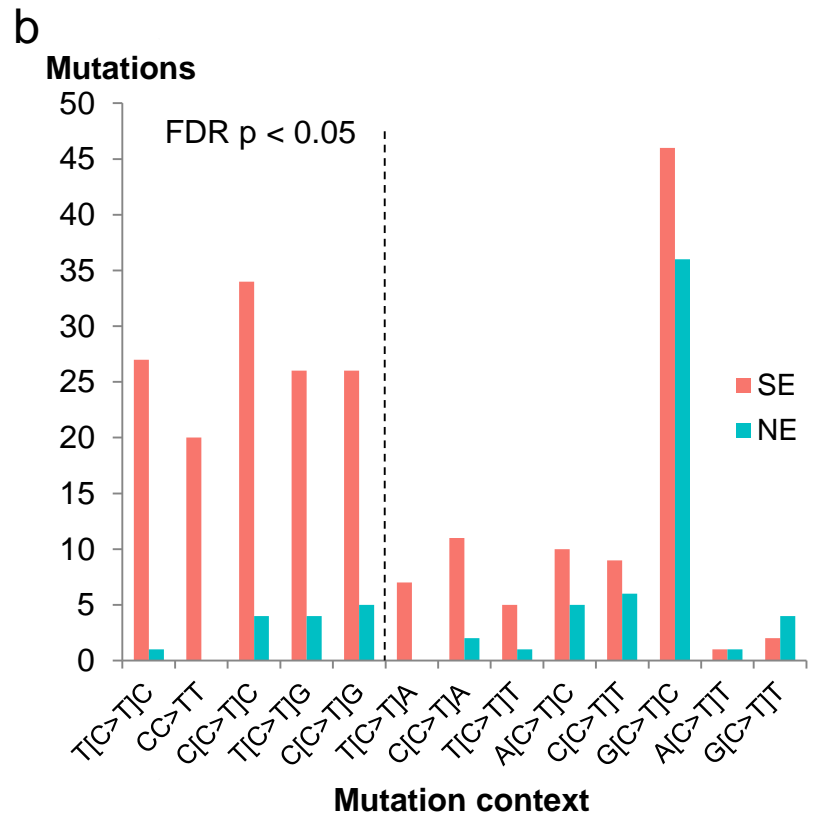
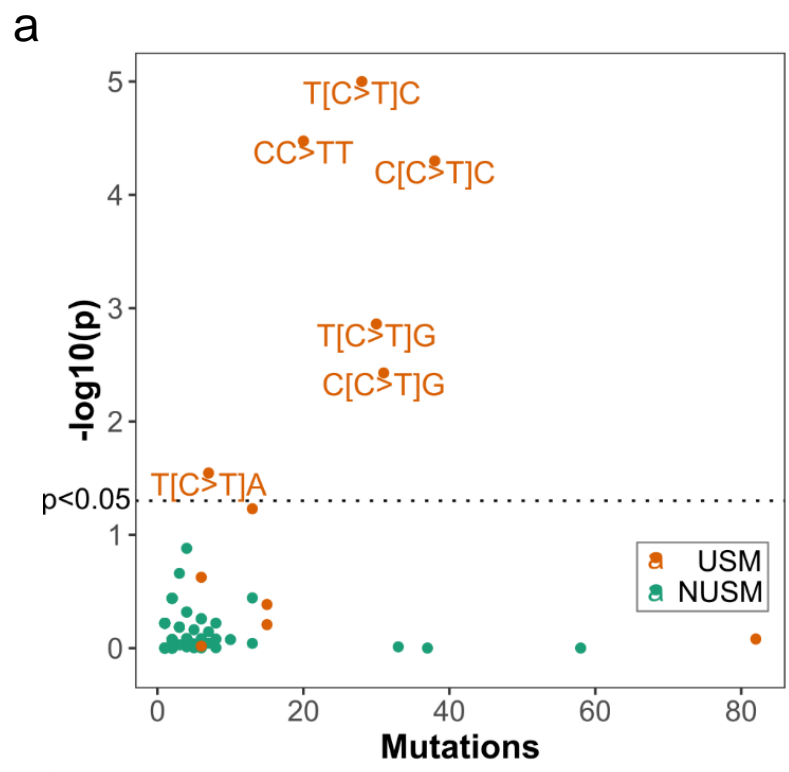


**Figure 6. Clonal mutation burden correlates with skin cancer risk**

